S3.Pa - Draft Paper 2 (EACEF 2022) _ rev1

by Joko Purnomo

Submission date: 19-Aug-2022 11:30AM (UTC+0700)
Submission ID: 1884226309
File name: S3.Pa_-_Draft_Paper_2_EACEF_2022___rev1.pdf (1.78M)
Word count: 3990
Character count: 20088

The effects of various parameters in sensitivity analysis of plain concrete beam using Rigid Body Spring Model

J Purnomo[1,3,a*], A L Han[1], B S Gan[2], D Hardjito[3]

[1]Department of Civil Engineering, Diponegoro University, Semarang, Indonesia
[2]Department of Architecture, Graduate School of Engineering, Nihon University, Koriyama, Japan
[3]Department of Civil Engineering, Petra Christian University, Surabaya, Indonesia
[a*]email: jpurnomo@students.undip.ac.id, jpurnomo@petra.ac.id

Abstract. The rigid body spring model (RBSM) is an alternative method to the finite element model (FEM) to solve continuum problems. The method has three main advantages, i.e., having a smaller local stiffness matrix, the ability to directly simulate cracks, and independent formulation of element types. Those advantages drove researchers to utilize the method to study a wide variety of civil engineering problems, such as cracks propagation, behaviour of mechanical anchors, freeze-thaw cycles, effects of corrosion, and steel to concrete bond. Although vast application of the method in civil engineering problems, specific research in key features of this model for plain concrete has not been done nor published. In this paper, sensitivity analysis on plain concrete beams using the method is performed. Parameters to consider in the analysis are boundary sizes, boundary element types, number of elements, crack mesh refinement, number of stages, and effects of half modelling. The effects of each parameter in RBSM are evaluated, including stress contour, cracks propagation, and load-displacement curves. The results show that the method's outcome is strongly dependent on mesh structure and displacement load step. Also, full modelling exhibits a more numerically stable behaviour compared to half modelling cases.

1. Introduction

The rigid body spring model (RBSM) is an alternative method to the finite element model (FEM) to solve continuum problems. The method was firstly introduced by Kawai (1) by discretizing the continuum domain into a finite number of rigid elements connected by springs at interfaces between elements. RBSM has key advantages compared to FEM, which has a smaller local stiffness size and thus shorter running time can be expected in simulating nonlinear cases (2), the ability to directly simulate crack since it is a discrete model (3), formulation independency regardless of element types, and compatibility with Voronoi mesh which can reduce bias to cracks propagation (4). In FEM, one method to simulate cracks is by introducing specific location for the cracks known as discrete crack approach (5). In the RBSM, these cracks can occur at arbitrary locations in the domain as the yield stress state is achieved. In its early implementation, the method was successfully employed to simulate the collapse of beams and plates (3), vibration analysis of structural elements and simple portal structure, slope stability, as well as tectonic plate movement (6).

Recently, RBSM has been explored to simulate a wide variety of civil engineering problems, including cracks propagation, behaviour of mechanical anchors, freeze-thaw cycles, effects of corrosion, and steel to concrete bond. Wang et al. (7) successfully simulated the cracks propagation on concrete under alkali-silica reaction. Karam et al. (8) used the model with Voronoi mesh to minimize bias on concrete cracks pattern. Mousavi et al. (9) reported the pull-out capacity of post-installed

anchors in concrete. Wang et al. (10) confirmed that concrete exposed to freeze-thaw cycles increased in static strength but conversely in fatigue performance. Jiradilok et al. (11) showed that confining steel can help increasing bond capacity between steel and concrete as well as slowing down cracks propagation rate in concrete.

Vast application of the method in solving engineering problems had been done. Nevertheless, specific research to study the sensitivity of the model on various parameters on plain concrete beam has not been done nor published. This research paper aims to present a sensitivity analysis of RBSM based on various parameters, including boundary sizes, boundary element types, number of elements, crack mesh refinement, number of stages, and effects of half modelling. Results of this research will be an important insight into the model and thus its optimal use for more sophisticated problems can be achieved. The results will be presented in the form of stress contours, cracks pattern, and load-displacement curves.

2. Rigid Body Spring Model

In RBSM, domain is discretized into finite number of rigid elements and connected via normal and shear springs at elements' contact line. Figure 1 shows the kinematics of rigid elements in RBSM. Elements' centroids are denoted by x_{Gi} ang y_{Gi}, respectively. Each element has three degrees of freedom to incorporate horizontal translation (u_i), vertical translation (v_i), and rotational movement (θ_i).

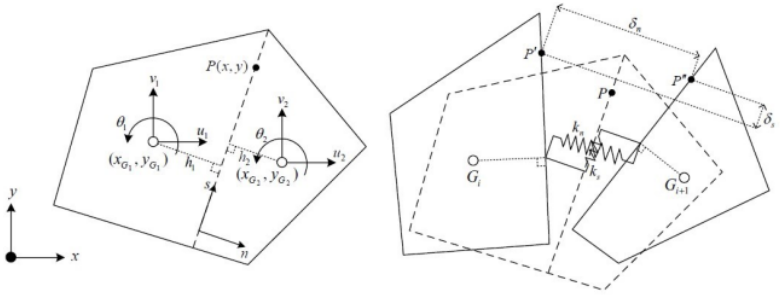

Figure 1. Kinematics of rigid elements in RBSM

Point P is arbitrary point locating at the contact line of the two elements. As the elements move, P will separate as P' and P" attached to each element. Global displacement of element's centroid (u_i) can be represented locally as the displacement of springs (U_i and V_i) as in equation (1). The stiffness of normal (k_n) and shear (k_s) spring can be calculated via equation (2), where E_c is modulus of elasticity, υ_c is Poisson's ratio, and h is the distance between two centroids and is orthogonal to line of contact. Further, normal (σ_n) and shear stress (τ_s) can be evaluated using equation (3) with ε_n and γ_s denote normal and shear strain, respectively. Further derivation of the equations is identical to those in FEM.

$$\begin{aligned} U_i &= u_i - (y - y_{Gi})\theta_i \\ V_i &= v_i + (x - x_{Gi})\theta_i \end{aligned} \tag{1}$$

$$k_n = \left(\frac{E_c}{1-\upsilon_c^{\,2}}\right)\frac{1}{h} \quad , \quad k_s = \left(\frac{E_c}{1+\upsilon_c}\right)\frac{1}{h} \tag{2}$$

$$\sigma_n = \left(\frac{E}{1-\upsilon^2}\right)\varepsilon_n \quad , \quad \tau_s = \left(\frac{E}{1+\upsilon}\right)\gamma_s \tag{3}$$

3. Constitutive Material Model

Figure 2 shows the material model for concrete and modified Mohr-Coulomb criteria. In compression, the material has initial stiffness of E_c until F_{c1} then the second stiffness is taken as βE_c until the stress

reaches F_{c2}. After reaching F_{c2}, the material behaves constantly until the strain reaches ε_{cu}. Beyond this strain, the stress drops linearly to $0.2F_c$ at $2\varepsilon_{cu}$. In tension, the material behaves linearly until reaching its ultimate tensile stress F_t then the stress released to zero following linear softening model.

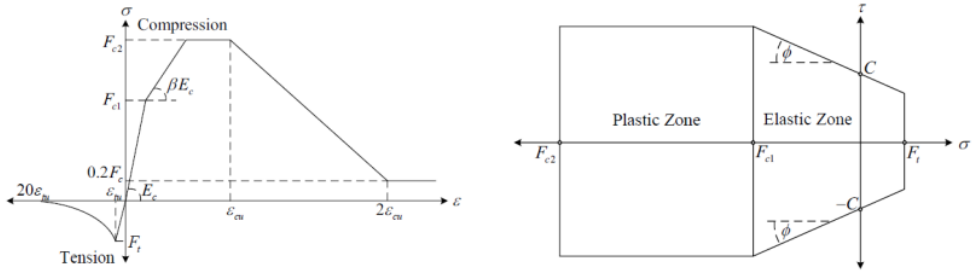

(a) (b)

Figure 2. Concrete material model (a), modified Mohr-Coulomb criteria (b)

The modified Mohr-Coulomb criteria were adopted to consider material yielding under the combination of normal and shear stresses. The shear stress equation based on original Mohr-Coulomb criteria is shown in equation (4), which τ, ϕ, and c denotes shear stress, friction angle, and cohesive stress, respectively. Further, the yield function of shearing slip (f) is defined as in equation (5). Details of material properties can be found in Table 1. It is worth noting that the constants correspond to failure criteria is adopted from recommended values by Yamamoto et al. (12).

$$\tau = \sigma \tan\phi + c \tag{4}$$

$$f = \tau^2 + (C - \sigma \tan\phi)^2 \tag{5}$$

Table 1. Material properties of concrete.

Parameter	Notation	Value	Unit
Poisson's ratio	υ_c	0.2	-
Cohesive stress	c	4.2	MPa
Friction angle	ϕ	37	°
Ultimate tensile stress	F_t	3.86	MPa
Tensile softening coef. 1	C_1	1.05	-
Tensile softening coef. 2	C_2	-350.88	-
Ultimate tensile strain	ε_{tu}	0.00015	-
Ultimate compressive stress	F_c	30	MPa
Modulus of elasticity	E_c	25,700	MPa
Second stiffness factor	β	0.5	-
Ultimate compressive strain	ε_{cu}	0.003	-

4. Sensitivity Analysis Model

Figure 1 shows the geometry of plain concrete beam. As an additional detail, the thickness of the beam is 100 mm. In the model, the beam is defined as simply supported beam and is loaded by displacement loading at third span. Parameters to be consider in this research are listed in Table 2. More details on the parameters for each model category can be found in following subsections.

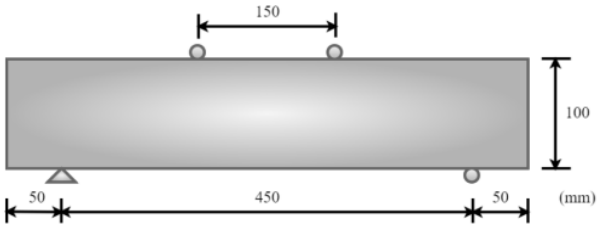

Figure 3. Geometry of plain concrete beam

Table 2. Parameters considered in sensitivity analysis.

Parameter	Model code
Boundary size	BS
Boundary element type	BT
Number of elements (full model)	NE
Crack mesh refinement	CM
Number of stages	SG
Half model	HF

4.1. Boundary elements size and types

Boundary elements size and types are important parameters on modelling continuum problems. In this research, boundary element size is defined as the length of boundary elements' edge that is in contact with model domain. This value is taken as ratio varies between 0.1 to 0.5 with respect to the minimum dimension of the model, i.e., the height. Meanwhile, the boundary element types refer to the number of nodes in the element. Table 3 shows the parameters of BS and BT-models. Negligible differences in total number of elements are shown in BS-2 and BS-4 model due to constraint in mesh generator tool. Model mesh of BS-3 and BT-8 can be seen in figure 4.

Table 3. Detail parameters of BS and BT-models.

Model	h_e	n_e	b_s	b_t	d_L
BS-1	20	714	10	4	0.0025
BS-2	20	710	20	5	0.0025
BS-3	20	714	30	6	0.0025
BS-4	20	710	40	7	0.0025
BS-5	20	714	50	8	0.0025
BT-6	20	714	30	6	0.0025
BT-8	20	714	30	8	0.0025

h_e = maximum size of elements (mm)
n_e = number of elements
b_s = boundary size (mm)
d_L = displacement load step (mm)
b_t = boundary types (n-nodes element)

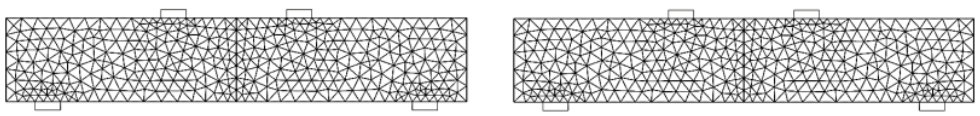

(a) (b)

Figure 4. Model mesh for BS-3 (a) and BT-8 (b)

4.2. Number of elements and half modelling

It is commonly understood that modelling continuum problems using finer mesh will yield into a more realistic result. However, excessive mesh refinement often cannot give meaningful results compared to a coarse mesh. Thus, investigating the effects of meshing density can be especially useful before applying the method to a more sophisticated problem. On the other hand, modelling only part of the model can be also useful when dealing with problems with field concentration. Table 4 resumes the parameters of NE and HF-models. The HF-models are half of those of NE-models. Therefore, based on the meshing, the NE-models are symmetrical, while the HF-models are nonsymmetric models, but the symmetry conditions are provided by the boundary conditions at symmetry line. Example model mesh of NE-0600 and HF-0300 can be observed in figure 5.

Table 4. Detail parameters of NE and HF-models.

Model	h_e	n_e	d_L	Model	h_e	n_e	d_L
NE-0156	40	156	0.0025	HF-0078	40	78	0.0025
NE-0256	30	256	0.0025	HF-0128	30	128	0.0025
NE-0600	20	600	0.0025	HF-0300	20	300	0.0025
NE-1032	15	1032	0.0025	HF-0516	15	516	0.0025
NE-2288	10	2288	0.0025	HF-1144	10	1144	0.0025
NE-4204	7.5	4204	0.0025	HF-2102	7.5	2102	0.0025
NE-9348	5.0	9348	0.0025	HF-4674	5	4674	0.0025

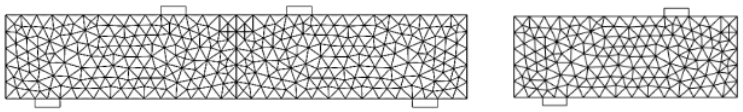

(a) (b)

Figure 5. Model mesh for NE-0600 (a) and HF-0300 (b)

4.3. Crack mesh refinement

Cracks propagation is one aspect that indicates how the model can capture the local failure during the analysis. In RBSM, cracks propagate directly at the elements' edges. The conditions suggest that the structure of the mesh may significantly affect the cracks pattern of the analysed model. Considering symmetric CM-model, the first crack is expected to form at the middle bottom of the beam. Thus, refining the area will yield a representative result. To compare the effect of symmetric and nonsymmetric mesh models, a predefined first crack location is proposed in the CM-P-models. The details parameters of both models can be found in table 5, while the mesh density of each model can be seen in figure 6.

Table 5. Detail parameters of CM and CM-P-models.

Model	h_e	n_e	t_{cr}	h_{cr}	s_{cr}	Sym.	d_L
CM-00	20	600	-	-	-	yes	0.0025
CM-10	20	714	10	-	-	yes	0.0025
CM-05	20	1124	5	-	-	yes	0.0025
CM-P-5-5	20	628	-	5	5	no	0.0025
CM-P-10-5	20	654	-	10	5	no	0.0025
CM-P-10-10	20	588	-	10	10	no	0.0025

t_{cr} = mesh size at middle bottom of the beam and upward along symmetry line
h_{cr} = height of predefined first crack (mm)
s_{cr} = mesh size at predefined first crack (mm)

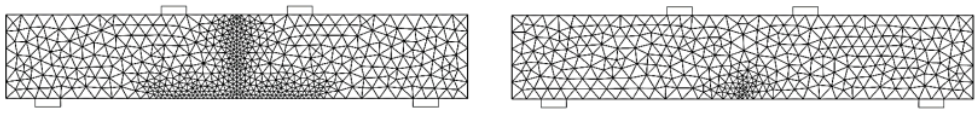

(a) (b)

Figure 6. Model mesh for CM-05 (a) and CM-P-10-5 (b)

4.4. Number of stages

Number of stages corresponds to the load applied in the model. Increasing the number of stages mean refining the load step, and vice versa. Parameterizing number of stages is selected because it is easier to apply and, in certain cases, selecting the load step first can yield to undesirable number of converged outputs. The model considered in this subsection has the same parameters to those of NE-0600 model with varying number of stages as shown in table 6.

Table 6. Detail parameters of SG-models.

Model	h_e	n_e	n_s	d_L
SG-0010	20	600	10	0.02500
SG-0050	20	600	50	0.00500
SG-0100	20	600	100	0.00250
SG-0500	20	600	500	0.00050
SG-1000	20	600	1000	0.00025
SG-5000	20	600	5000	0.00005

n_s = number of stages

5. Results and Discussion

The results comprise stress contours, plasticity index contours, and load-displacement curves. The stress contours can be used to examine the internal response of the model due to applied load. Stress contour of selected models with notable findings will be presented. Plasticity index contours show plastic state of the material and correspond directly to cracks formation. The last but not the least, load-displacement curves will show the overall behaviour of each model regarding the initial stiffness, ultimate load, and ductility.

5.1. Stress contour

Most models result in identical stress contour, and thus only important findings regarding stress contour are shown. Figure 7 shows the normal stress contour for model NE-0156, NE-0600, NE-4204, and NE-9348. For the consecutive models, maximum compressive stresses are 3.10, 1.52, 1.63, and 5.40 MPa, while maximum tensile stresses are 1.25, 1.06, 1.02, and 2.04 MPa. It is clearly depicted in figure 7(a), (b), and (c), as the mesh is refined, stress concentration occurs around the location where cracks form and propagate. Meanwhile, figure 7(d) shows different stress concentration following distinct cracks pattern. The cracks pattern differs from the first three models because as the mesh is refined, the location of first crack might change, and thus the cracks propagation.

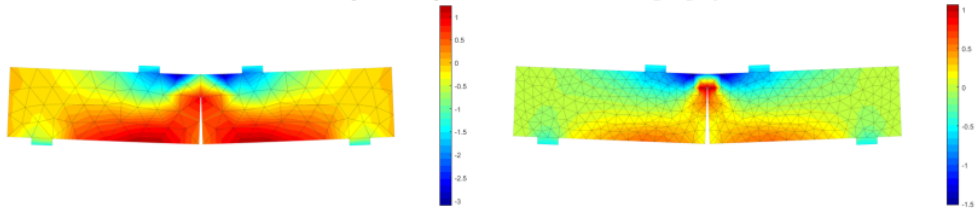

(a) (b)

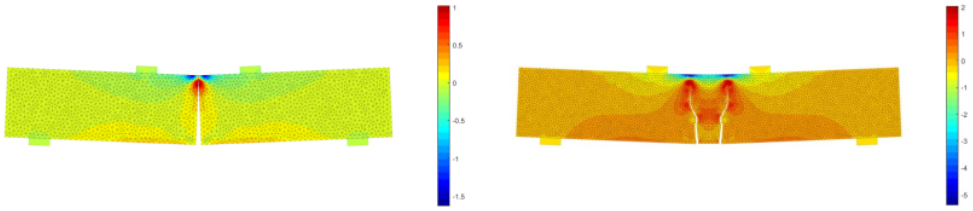

(c) (d)

Figure 7. Normal stress contour of NE-0156 (a), NE-0600 (b), NE-4204 (c), and NE-9348 (d) model

5.2. Plasticity index

Figure 8 shows normalized plasticity index contour for model CM-00, CM-05, CM-P-5-5, and CM-P-10-5. As expected from symmetrical mesh models (CM), the first crack occurs at middle bottom of the beam and propagates upward following the symmetry line of the beam. Nonsymmetric mesh models (CM-P) result in a more rational cracks pattern. The predefined first crack location can lead the model to form first crack at the location, and the nonsymmetric mesh will guide the cracks propagation to a more realistic manner. Both CM-P-5-5 and CM-P-10-5 result in satisfactory cracks pattern.

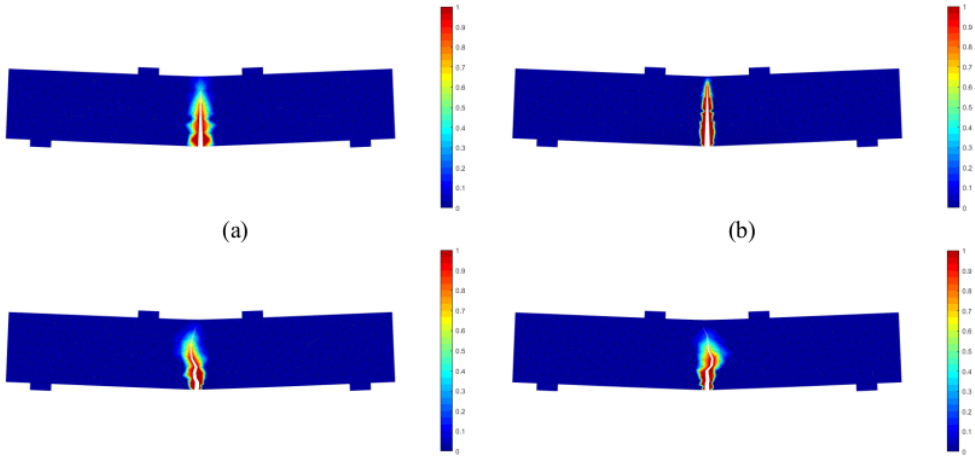

(a) (b)

(c) (d)

Figure 8. Plasticity index for CM-00 (a), CM-05 (b), CM-P-5-5 (c), CM-P-10-5(d)

5.3. Load-displacement curves

Figure 9 shows the load-displacement curves of BS and BT-models. It clearly shows that increasing the boundary elements size is insignificant to ultimate load but increasing the initial stiffness of the model. This is because as the size of the boundary elements increased, the clear span of the model is reduced. On the other hand, different boundary element types do not affect the overall behaviour of the models. This is because, in RBSM, elements are rigid and thus element distortion is not allowed. Any elements with the same boundary conditions will serve the same roles in the model.

Figure 10 reveals the load-displacement curves of NE and HF-models. The first notable finding in NE-models is that refining the mesh insignificantly alter the initial stiffness of the model. However, as the mesh is refined, the ultimate load drops until certain number of elements that the drop rate becomes negligible as shown by NE-2288, NE-4204, and NE-9348 model. Also, an extra coarse model (NE-0156) exhibits ductility while other models do not. Both half and full modelling result in

the identical ultimate load and initial stiffness. Further, from the curves, it can be understood that full modelling is more numerically stable than half modelling after peak load is achieved.

Figure 11 displays the load-displacement curves of SG and CM-models. Increasing the number of stages or decreasing the load step will yield a more representative outcomes, while smaller number of stages will result in rough load-displacement curve. Dividing the analysis into larger number of stages will not produce a substantial finer result with the excessive computational efforts. Based on the curves, the optimal number of stages in this research lies between fifty to one hundred stages. Meanwhile, refining the mesh around the expected cracks (CM) will slightly increase the stiffness and drop the ultimate load. This is due to the increase in number of elements when mesh refinement is applied. Nonsymmetric models (CM-P) with predefined first crack location can also yield reasonable results compared to those of CM-models. This finding implies that the method can be used to analysed nonsymmetric models with any predefined first crack location as needed.

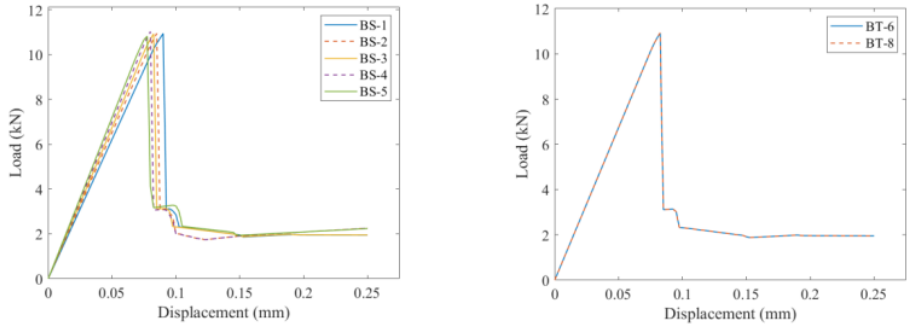

(a) (b)

Figure 9. Load-displacement curve of BS-models (a) and BT-models (b)

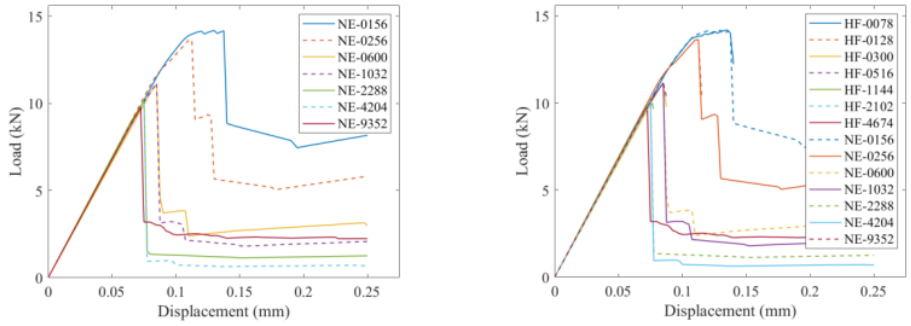

(a) (b)

Figure 10. Load-displacement curve of NE-models (a) and HF-models (b)

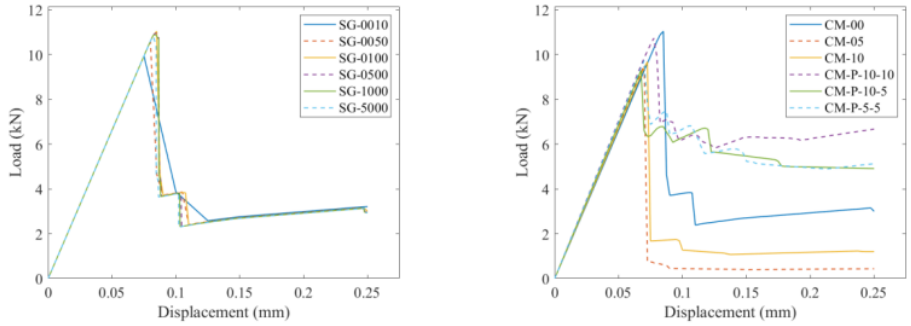

(a) (b)

Figure 11. Load-displacement curve of SG-model (a) and CM-model (b)

5.4. Experimental Results and Validation

Figure 12 shows the crack location of BC1, BC2, and BC3 specimen. Based on the observations, the location of the cracks was 190, 247, and 272 mm from the left support for BC1, BC2, and BC3, respectively. The values were all in the middle third span of the beam, i.e., in the range of 150 to 300 mm. The ultimate load for the specimens were 8.76, 8.81, and 8.55 kN. Average concrete compressive strength was 35.82 ± 1.15 MPa. Based on the experimental results, parameters in **Table 1** is adjusted to model the specimens as is shown in **Table 7**.

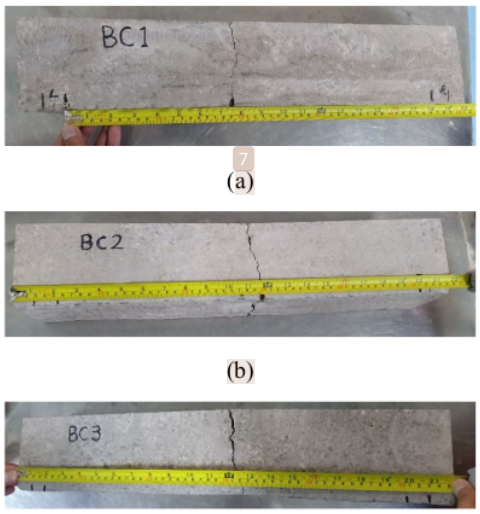

(a)

(b)

(c)

Figure 12. Crack location of BC1 (a), BC2 (b), and BC3 (c) specimen

Table 7 shows material properties of tested specimens. All values are identical, except for the ultimate tensile stress that is calculated based on modulus of rupture of concrete. Each specimen was modelled by introducing mesh at the crack location as studied in sensitivity analysis model CM-P-10-5, boundary element size of 30 mm, maximum stages of 100, displacement load step of 1/100 the ultimate displacement of tested specimens, and the boundary conditions are hinge and roller. Modulus of elasticity of the concrete is adjusted as the values shown in the table are based on cylindrical

concrete compressive test. After iterative process, the modulus elasticity is equal to 0.235, 0.195, and 0.185 times the modulus elasticity for specimen BC1, BC2, and BC3, respectively. The load displacement curves comparison between models and tested specimens is shown in **Figure 13**. Visually, the results are satisfactory following the iterative simulation. The ultimate load of each model is 8.78, 9.58, and 8.93 kN. These values 0.23%, 8.74%, and 4.44% greater than those obtained from tests. Crack pattern of the models are shown in **Figure 14**. Introducing mesh at location of actual crack can result in correct crack initiation and propagation as in the test. Nevertheless, the model cannot display crack propagation to reach top fibre of concrete beam due to computational instability. This is notable in the figure as the load undergoes sudden drop. The cracks pattern showed by the model differ from those from test results due to unstructured mesh. The result can be enhanced by reducing the element size or increasing the number of elements.

Table 7. Concrete material properties of tested specimens

Parameter	Notation	BC1	BC2	BC3	Unit
Poisson's ratio	υ_c	0.2	0.2	0.2	-
Cohesive stress	c	4.2	4.2	4.2	MPa
Friction angle	ϕ	37	37	37	°
Ultimate tensile stress	F_t	3.94	3.97	3.85	MPa
Tensile softening coef. 1	C_1	1.05	1.05	1.05	-
Tensile softening coef. 2	C_2	-350.88	-263.16	-263.16	-
Ultimate tensile strain	ε_{tu}	0.00015	0.00015	0.00015	-
Ultimate compressive stress	F_c	35.82	35.82	35.82	MPa
Modulus of elasticity	E_c	28,129	28,129	28,129	MPa
Second stiffness factor	β	0.5	0.5	0.5	-
Ultimate compressive strain	ε_{cu}	0.003	0.003	0.003	-

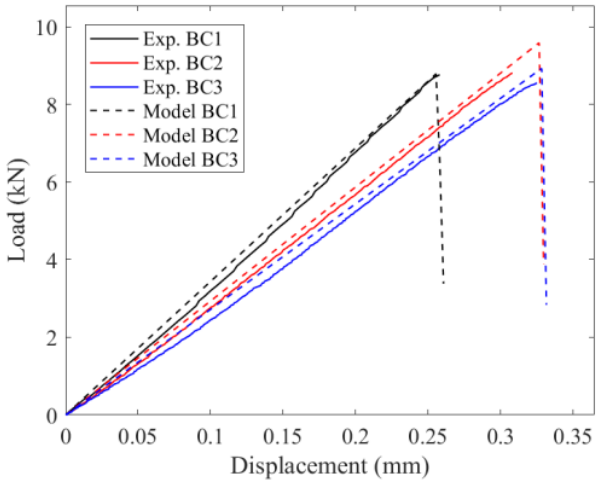

Figure 13. Load-displacement curves comparison between models and test results

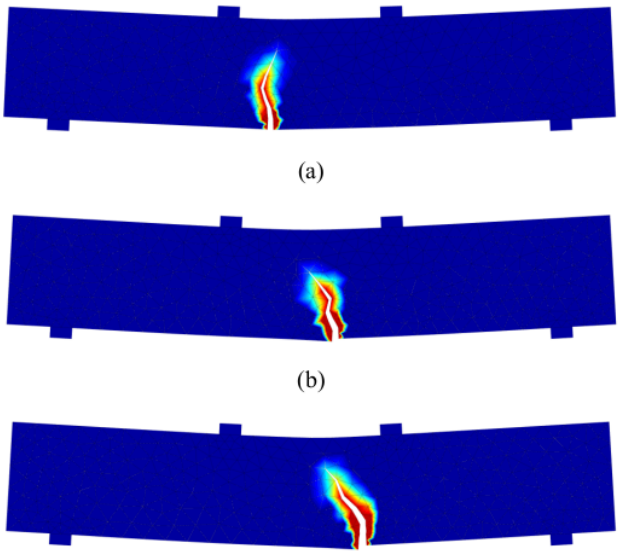

(a)

(b)

(c)

Figure 14. Crack pattern of model BC1 (a), BC2 (b), and BC3 (c)

6. Conclusion

Based on the results and discussion in prior sections, the following conclusions can be drawn. Firstly, the results obtained from RBSM strongly depends on meshing as the cracks propagation will follow the mesh. Secondly, denser mesh model will result in a significant lower ultimate load and slightly higher stiffness. Thirdly, boundary size affects the initial stiffness but insignificantly affects ultimate load. Different element types for boundary elements do not influence the overall behaviour of the model. Moreover, selecting large number of stages will not result in substantial load-displacement curve. A range of fifty to one hundred stages is recommended in this research. Using all recommended values, the model validation to experimental results shows that modulus of elasticity of concrete based on cylindrical concrete compressive test need to be adjusted in the range of 0.185 to 0.225 times. An initial ratio of 0.2 might be good starting values in the iterative analysis. The future work to develop this model is to establish bond model for composite and structural strengthening materials.

7. Acknowledgement

This study was financially supported by Faculty of Planning and Civil Engineering, Petra Christian University, No. 001/SK/FTSP/UKP/2022. The authors would like to express appreciation to the support.

8. References

1. Kawai T. New beam and plate bending elements in finite element analysis. Seisan Kenkyu. 1976;28(9):K3/8.
2. Kawai T. A new element in discrete analysis of plane strain problem. Seisan Kenkyu. 1977;29(4):204–7.
3. Kawai T. New element models in discrete structural analysis. J Soc Nav Archit Japan. 1977;52(5):174–80.
4. Bolander JE, Saito S. Fracture analyses using spring networks with random geometry. Eng

Fract Mech. 1998 Nov;61(5–6):569–91.
5. Tudjono S, Lie HA, As'ad S. Reinforced Concrete Finite Element Modeling based on the Discrete Crack Approach. Civ Eng Dimens. 2016;18(2):72–7.
6. Kawai T. New discrete models and their application to seismic response analysis of structures. Nucl Eng Des. 1978;48:207–29.
7. Wang Y, Meng Y, Jiradilok P, Matsumoto K, Nagai K, Asamoto S. Expansive cracking and compressive failure simulations of ASR and DEF damaged concrete using a mesoscale discrete model. Cem Concr Compos [Internet]. 2019;104(May):103404. Available from: https://doi.org/10.1016/j.cemconcomp.2019.103404
8. Karam MS, Yamamoto Y, Ikuma K, Nakamura H. Development of Voronoi meshing method capable of reproducing arbitrary shape for RBSM analysis. Annu Proc Concr Eng. 2020;42(2):541–6.
9. Mousavi Siamakani SY, Jiradilok P, Nagai K, Sahamitmongkol R. Discrete mesoscale analysis of adhesive anchors under tensile load taking into account post-installed reinforcement. Constr Build Mater [Internet]. 2020 Nov;262:120778. Available from: https://doi.org/10.1016/j.conbuildmat.2020.120778
10. Wang Z, Gong F, Ueda T. Modeling and Simulation on Static and Fatigue Behaviors of Intact and Frost Damaged Concrete with Ice-strengthening Effects. J Adv Concr Technol. 2021;19(April):346–58.
11. Jiradilok P, Avadh K, Nagai K. Simulation of effect of strirrup confinement on residual bond performance of corroded RC by 3D RBSM. Seisan Kenkyu. 2020;72(4):2–4.
12. Yamamoto Y, Nakamura H, Kuroda I, Furuya N. Simulation of crack propagation in RC shear wall using a 3D rigid-body-spring model with random geometry. In: Proceedings of the 8th International Conference on Fracture Mechanics of Concrete and Concrete Structures, FraMCoS 2013. 2013. p. 381–92.

S3.Pa - Draft Paper 2 (EACEF 2022) _ rev1

ORIGINALITY REPORT

5%	2%	4%	%
SIMILARITY INDEX	INTERNET SOURCES	PUBLICATIONS	STUDENT PAPERS

PRIMARY SOURCES

1	Watanabe, K.. "Biomechanical analysis of radial wedge osteotomy for the treatment of Kienbock's disease", Journal of Hand Surgery, 199307 Publication	1%
2	"High Tech Concrete: Where Technology and Engineering Meet", Springer Science and Business Media LLC, 2018 Publication	<1%
3	eprints.undip.ac.id Internet Source	<1%
4	"Computational Mechanics '86", Springer Science and Business Media LLC, 1986 Publication	<1%
5	Soonho Kim, Yun Sik Jang, Taekgeun Oh, Seung Kyun Lee, Doo-Yeol Yoo. "Effect of crack width on electromagnetic interference shielding effectiveness of high-performance cementitious composites containing steel and carbon fibers", Journal of Materials Research and Technology, 2022	<1%

Publication

6	Wei-Xin Ren, Xiangguang Tan, Zhaochang Zheng. "Nonlinear analysis of plane frames using rigid body-spring discrete element method", Computers & Structures, 1999 Publication	<1 %
7	eprints.gla.ac.uk Internet Source	<1 %
8	Lipei Song, Zhen Zhou, Xueyan Wang, Xing Zhao, Daniel S. Elson. "Simulation of speckle patterns with pre-defined correlation distributions", Biomedical Optics Express, 2016 Publication	<1 %
9	S. - W. HAN, S. - W. KIM, S. KUMAI. "Effects of solidification structure on tear resistance of Al–7% Si–0.4% Mg cast alloys", Fatigue & Fracture of Engineering Materials & Structures, 2004 Publication	<1 %
10	dspace.vutbr.cz Internet Source	<1 %
11	Casolo, S.. "Seismic analysis and strengthening design of a masonry monument by a rigid body spring model: The ''Maniace Castle'' of Syracuse", Engineering Structures, 200907 Publication	<1 %

12	Nenad Bićanić. "Discontinuous modeling of cohesive-frictional blocky materials", European Journal of Environmental and Civil Engineering, 2011 Publication	<1 %
13	Seyed Yaser Mousavi Siamakani, Raktipong Sahamitmongkol. "Post-installed anchors in concrete strengthened by post-installed reinforcement under tensile load", European Journal of Environmental and Civil Engineering, 2021 Publication	<1 %
14	Taito Miura, Stéphane Multon, Yuichiro Kawabata. "Influence of the distribution of expansive sites in aggregates on microscopic damage caused by alkali-silica reaction: Insights into the mechanical origin of expansion", Cement and Concrete Research, 2021 Publication	<1 %
15	dspace.cvut.cz Internet Source	<1 %
16	www.jstage.jst.go.jp Internet Source	<1 %

Exclude quotes	Off	Exclude matches	Off
Exclude bibliography	On		